26

Development of a LCD Photomask Based Desktop Manufacturing System

Ren C. Luo[1] and Jyh-Hwa Tzou[2]
[1]*Department of Electrical Engineering, National Taiwan University*
[2]*Department of Aeronautical Engineering, National Formosa University*
Taiwan, R. O. C.

1. Introduction

Desktop manufacturing refers to various rapid prototyping (RP) techniques where three-dimensional components are directly built, layer-by-layer, from a computer data description or computer aided design (CAD) file. Due to their ability and relative ease in transforming a conceptual design into a physical model, desktop manufacturing technologies have met escalating demand in the industry for shortening new product development cycle time. The layer-by-layer fabrication methodology also allows complex models to be made with ease.

In the desktop manufacturing processes, the geometry of the object to be manufactured can be obtained from computer aided design (CAD) model data, an existing object (through Reverse engineering) (Puntambenker et al., 1994) (Soboh et al., 1994) (Chua Chee Kai, 1994) or mathematical data (e.g., surface equations) (Ren C Luo & Yawei Ma, 1995). Prashant et al. (Prashant Kulkarni et al., 2000) had reviewed many process planning techniques in layer manufacturing. Most desktop manufacturing systems accept model data described in an intermediate file format called the .STL format. This file format approximates the original model geometry using a series of triangular facets.

After loading a .STL model, a slicing procedure is then applied to the tessellated model. In this process, the model is intersected with a set of horizontal planes to create a series of cross sections, or slices, comprised of contours that represent the material boundaries of the part to be generated. The contours are subsequently used to generate the NC tool paths for the desktop manufacturing system.

There are many commercial RP systems available on the market today such as InVision (3D Systems Corporation), Objet (Objet Geometries Ltd.), Perfactory (Envisiontec Inc.), stereolithography (SLA) (3D Systems Corporation) and fused deposition modeling (FDM) (Stratasys, Inc.). The InVision 3-D printer combines 3D Systems' multi-jet modeling (MJM) printing technology with an acrylic photopolymer model material. The Objet's Polyjet technology works by jetting photopolymer materials in ultra-thin layers (0.016 mm) onto a build tray, layer by layer, until the part is complete. The Perfactory RP system uses a photomonomer resin and a DLP projector to polymerize 3D finished parts. The stereolithography (SLA) and fused deposition modeling (FDM) are old RP processes. Both the laser beam of SLA system and the thermal extrusion head of FDM system generate 2D cross sectional areas using one-dimensional tool paths. The disadvantages of these systems

Source: Motion Control, Book edited by: Federico Casolo,
ISBN 978-953-7619-55-8, pp. 580, January 2010, INTECH, Croatia, downloaded from SCIYO.COM

are lower speed, the requirement for an expensive XYZ table and 3 axes motion control system. Another old RP process, Solid Ground Curing (SGC) (Cubital Ltd.), involves creating a temporary photomask of each layer, applying a thin coating of photopolymers and exposing the layer to a burst of ultraviolet light to cure it. Because the cross sections of one layer are cured at the same time, the SGC system has a faster build speed. But the mechanism of the SGC system is complex, and the price is very expensive.

The purpose of this paper is to develop a low cost desktop manufacturing system. We use a liquid crystal display (LCD) panel as a photomask(Luo, R. C. et al., 2000). With the bottom exposure method, the image of the LCD photomask is calculated from the sliced data. The desktop manufacturing system has the advantages of low cost, compactness and requiring no special physical support, making it suitable for use in an office.

S. C. Ventura et al. (S. C. Ventura et al., 1996) developed a Direct Photo Shaping process for the fabrication of functional ceramic components layer by layer. Each layer is photoimaged by a LCD or a digital light processing (DLP) projection system. Young, J. S. et al. (Young, J. S. et al. , 1999) described a novel device for producing 3D objects that has been developed using an LCD as a programmable, dynamic mask and visible light to initiate photopolymerization. Monneret, Serge et al. (Monneret, Serge et al. , 2002) presented a new process of microstereolithography to manufacture freeform solid 3D micro-components with outer dimensions in the millimeter size range. Huang, Y. -M. et al. (Huang, Y. -M. et al., 2003) analyzed the shrinkage deformation of the mask type stereolithography process. Jiang, C. -P. et al. (Jiang, C. -P. et al., 2005) developed a Masked Photopolymerization Rapid Prototyping (MPRP) system using LCD panel as dynamic mask with an upper exposure skill.

2. LCD photomask based desktop manufacturing system

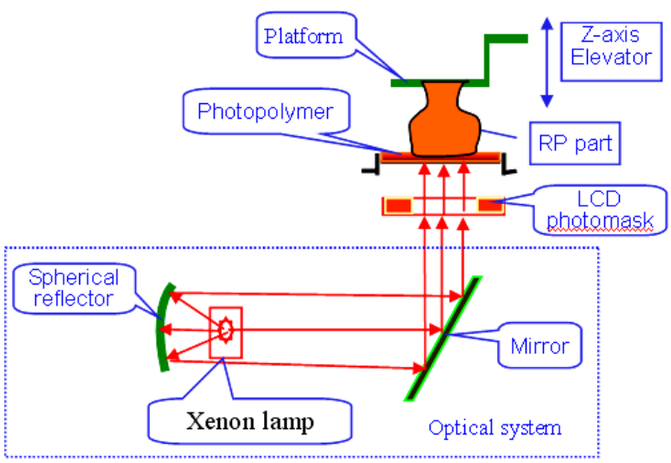

Fig. 1. Configuration of the LCD photomask based desktop manufacturing system

The LCD photomask based desktop manufacturing system structure is illustrated in Fig. 1. The hardware configuration of this system includes the LCD photomask, optical system, z-axis elevator and PC based control system. The optical system can generate parallel light passing through the LCD photomask to cure the photopolymer. The RP part is generated layer-by-layer and attached to a platform that rises as each successive layer is attached to the bottom-most face. The resin is deposited onto the transparent bottom plate. The platform

and previously built structure are lowered into the resin, leaving a liquid film between the part and the bottom plate that has the correct thickness for the next layer. The new layer is formed beneath the platform by exposing the LCD photomask. After the layer is finished, the platform is raised, separating the layer from the bottom plate, filling and wiping the resin and the process is repeated until all layers are fabricated. The completed RP part is then removed from the platform, post cured and finished, if needed.

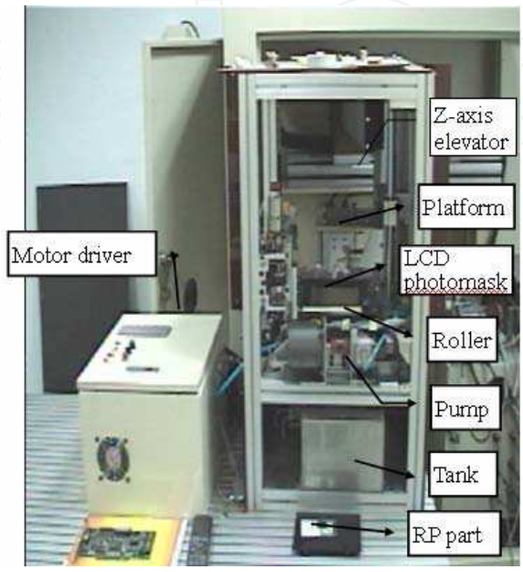

Fig. 2. Photo of the LCD photomask based desktop manufacturing system

The desktop manufacturing system architecture is illustrated in Fig. 2. The Z-axis elevator with a high precision ball screw is driven by an AC servomotor. A PC-based DSP motion controller is used to control the movement of the Z-axis elevator. The LCD photomask is connected to the VGA card of the computer.

The architecture of the proposed system includes five main components; 1) Data processing unit; 2) LCD photomask; 3) Optical system; 4) PC based DSP Motion Control System; 5) Z-axis elevator. The details of these components are as follows:

2.1 Data processing unit

The data processing unit performs the slicing procedure and the photomask generation process. The slicing procedure transforms the 3-D CAD model into a set of 2-D layer contours. According to this contour data, the photomask generation program exports the contour of each layer to the LCD photomask. Note that the region inside the contour is displayed in white color and the region outside the contour is displayed in black color.

2.2 LCD photomask

An LCD serves as a photomask which is used to display layer contours. The light source emits parallel light upwardly through the transparent portions of the LCD photomask to expose and solidify the entire layer at once. As shown in Fig. 3, a 14.1-inch TFT (Thin Film Transistor) LCD with 1024x768 pixels is used herein. Each pixel is 0.28 mm in both width and length, yielding a photomask resolution of under 0.28 mm. An insulating membrane is located below the LCD photomask to insulate the resin from ultraviolet and heat produced

by the light source. Furthermore, the size of the RP part can be produced in this system is restricted by the size of the LCD panel used. If we can use larger LCD panel, the size of the RP part could be increased.

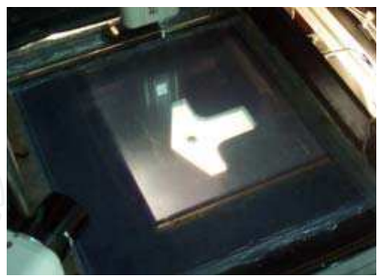

Fig. 3. The LCD photomask of the proposed system

2.3 Optical system:

The optical system strongly influences the system structure, forming method and building time for parts. The proposed system uses NAF-200N photo-curable liquid resin (Denken Engineering Co. Ltd., Japan), as the building material. NAF-200N solidifies under exposure to 680 nm visible light. A 275W xenon lamp serves as the light source. The optical spectrum of this xenon lamp, detected by a spectrometer, is shown in Fig. 4, where the spectral radiance is observed with maximum power at 736nm wavelength and a lot of energy at 680 nm. The experimental results confirm the ready solidification of NAF-200N under exposure to this xenon lamp. According to the experimental results, the layer thickness for one layer is 0.254mm. The curing time for one layer is 135 sec.

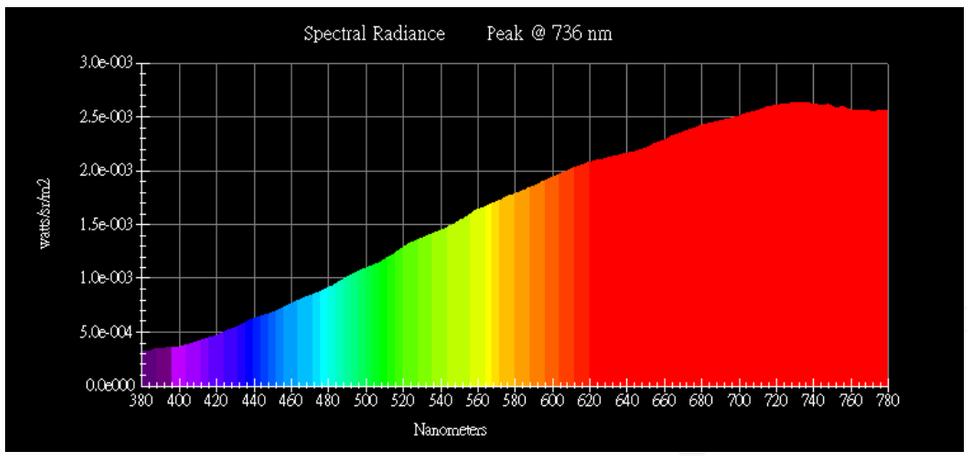

Fig. 4. The spectrogram of the 275W xenon lamp.

The optical system design is illustrated in Fig. 5(a). The actual structure is shown in Fig. 5(b).The proposed system uses plane-shaping instead of line-shaping. The visible light source is emitted from the bottom up to the part instead of from the top down in order to reduce the amount of resin wasted.

The ray tracing method is an important tool in geometrical optics. Matrix optics (Eugene Hecht, 2002) was used to design the RP machine optical system. A ray is described by its position and its angle with respect to the optical axis. The matrix form of several optical components can be shown as follows:

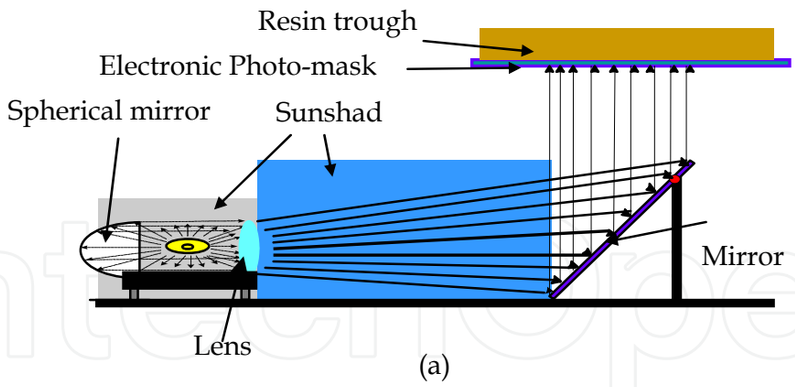

(a)

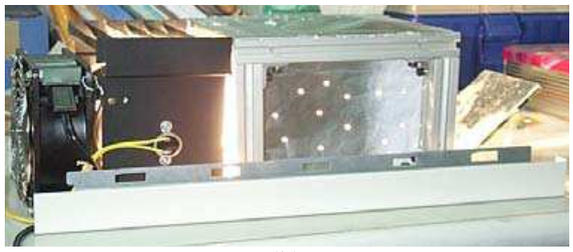

(b)

Fig. 5(a). The design of the curing light source; 5(b) Real structure of the curing light source

1. **Free – space propagation**

As shown in Fig. 6, a ray traversing a distance d is altered in accordance with $y_2 = y_1 + \theta_1 d$ and $\theta_2 = \theta_1$.

The ray-transfer matrix is $T = \begin{bmatrix} 1 & d \\ 0 & 1 \end{bmatrix}$, and $\begin{bmatrix} y_2 \\ \theta_2 \end{bmatrix} = \begin{bmatrix} 1 & d \\ 0 & 1 \end{bmatrix} \begin{bmatrix} y_1 \\ \theta_1 \end{bmatrix} = T \begin{bmatrix} y_1 \\ \theta_1 \end{bmatrix}$ (1)

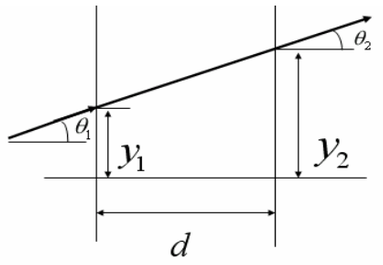

Fig. 6. Free – space propagation

2. **Transmission through a thin lens**

As shown in Fig. 7, the relation between θ_1 and θ_2 for paraxial rays transmitted through a thin lens of focal length f. Since the height remains unchanged $(y_2 = y_1)$, the refraction matrix of thin lens is $A = \begin{bmatrix} 1 & 0 \\ -\frac{1}{f} & 1 \end{bmatrix}$, and $\begin{bmatrix} y_2 \\ \theta_2 \end{bmatrix} = \begin{bmatrix} 1 & 0 \\ -\frac{1}{f} & 1 \end{bmatrix} \begin{bmatrix} y_1 \\ \theta_1 \end{bmatrix} = A \begin{bmatrix} y_1 \\ \theta_1 \end{bmatrix}$ (2)

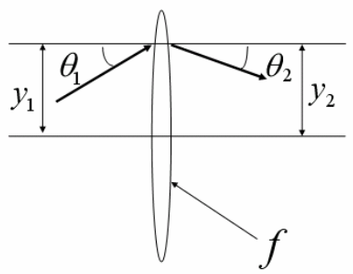

Fig. 7. Transmission through a thin lens

3. **Reflection from a planar mirror**

As shown in Fig. 8, the ray position is not altered $(y_2 = y_1)$, and we conclude that $\theta_2 = \theta_1$. The ray-transfer matrix is therefore the identity matrix $R = \begin{bmatrix} 1 & 0 \\ 0 & 1 \end{bmatrix}$, and

$$\begin{bmatrix} y_2 \\ \theta_2 \end{bmatrix} = \begin{bmatrix} 1 & 0 \\ 0 & 1 \end{bmatrix} \begin{bmatrix} y_1 \\ \theta_1 \end{bmatrix} = R \begin{bmatrix} y_1 \\ \theta_1 \end{bmatrix} \tag{3}$$

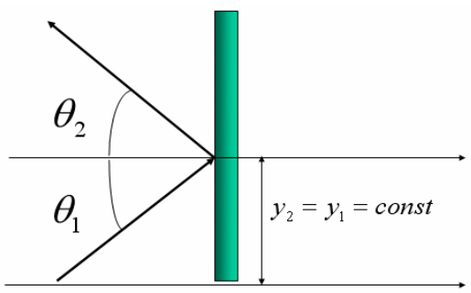

Fig. 8. Reflection from a planar mirror

4. **Reflection from a spherical mirror**

As shown in Fig. 9, the ray position is not altered $(y_2 = y_1)$. The reflection matrix of a spherical mirror is $S = \begin{bmatrix} 1 & 0 \\ -\frac{2}{R} & 1 \end{bmatrix}$, and

$$\begin{bmatrix} y_2 \\ \theta_2 \end{bmatrix} = \begin{bmatrix} 1 & 0 \\ -\frac{2}{R} & 1 \end{bmatrix} \begin{bmatrix} y_1 \\ \theta_1 \end{bmatrix} = S \begin{bmatrix} y_1 \\ \theta_1 \end{bmatrix} \tag{4}$$

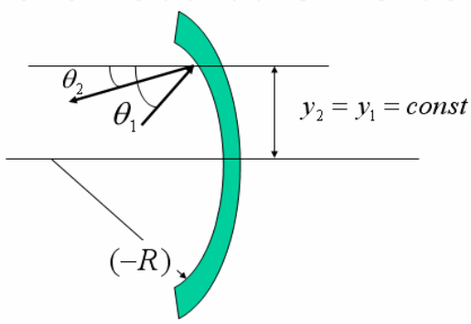

Fig. 9. Reflection from a spherical mirror

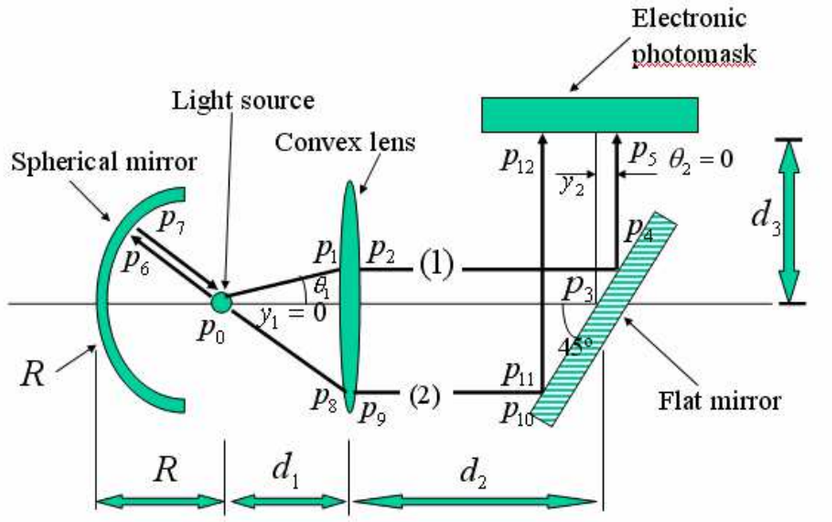

Fig. 10. The ray tracing diagram of the optical system of RP machine

The ray tracing diagram of the optical system of RP machine is shown in Fig. 10. The light source P_0 (xenon lamp) is located on the focus of the biconvex lens and on the center position of the spherical mirror. The ray emitted by light source P_0 can be divided into two parts, one [Ray trajectory (1)] transmits through the thin lens directly, and the other [Ray trajectory (2)] is reflected from the spherical mirror.

These two ray trajectories are discussed as follows:

- **Ray trajectory (1): P_0P_1 P_2 P_3 P_4 P_5**

The ray emitted from light source P_0, transmits through the thin lens. After reflecting the ray from the flat mirror, the reflected parallel light can be generated onto the LCD photomask position (P_5). The system matrix is then defined as:

$$M_1 = T_{54}R_{43}T_{32}A_{21}T_{10} = \begin{bmatrix} 1 & d_3 \\ 0 & 1 \end{bmatrix}\begin{bmatrix} 1 & 0 \\ 0 & 1 \end{bmatrix}\begin{bmatrix} 1 & d_2 \\ 0 & 1 \end{bmatrix}\begin{bmatrix} 1 & 0 \\ -\frac{1}{f} & 1 \end{bmatrix}\begin{bmatrix} 1 & d_1 \\ 0 & 1 \end{bmatrix} =$$

$$= \begin{bmatrix} 1-\frac{d_2}{f}-\frac{d_3}{f} & d_1+d_2\left(-\frac{d_1}{f}+1\right)-\frac{d_1d_3}{f}+d_3 \\ -\frac{1}{f} & -\frac{d_1}{f}+1 \end{bmatrix} \quad (5)$$

Where:

T_{10} = The ray-transfer matrix is from P_0 to P_1

A_{21} = The thin lens refraction matrix is from P_1 to P_2

T_{32} = The ray-transfer matrix is from P_2 to P_3

R_{43} = The reflection matrix of a planar mirror is from P_3 to P_4

T_{54} = The ray-transfer matrix is from P_4 to P_5

Thus the ray at point P_5 on the LCD photomask position is given by:

$$\begin{bmatrix} y_2 \\ \theta_2 \end{bmatrix} = M1 * \begin{bmatrix} y_1 \\ \theta_1 \end{bmatrix} = \begin{bmatrix} 1-\frac{d_2}{f}-\frac{d_3}{f} & d_1+d_2\left(-\frac{d_1}{f}+1\right)-\frac{d_1 d_3}{f}+d_3 \\ -\frac{1}{f} & -\frac{d_1}{f}+1 \end{bmatrix} \begin{bmatrix} y_1 \\ \theta_1 \end{bmatrix} \tag{6}$$

If d_1 = f and y_1 =0, equation (6) can be simplified as

$$\begin{bmatrix} y_2 \\ \theta_2 \end{bmatrix} = \begin{bmatrix} 1-\frac{d_2}{f}-\frac{d_3}{f} & f \\ -\frac{1}{f} & 0 \end{bmatrix} \begin{bmatrix} 0 \\ \theta_1 \end{bmatrix} \tag{7}$$

Consequently, $y_2 = f\ \theta_1$ and θ_2 =0 (8)

- **Ray trajectory (2): $P_0P_6\ P_7\ P_8\ P_9\ P_{10}\ P_{11}\ P_{12}$**

As shown in Fig.10, the ray emitted from light source P_0 is reflected by the spherical mirror. After the reflected ray is transferred through the thin lens and flat mirror, the parallel light can be generated onto the LCD photomask position (P_{12}). The system matrix is then defined as:

$$M2 = T_{12\cdot 11} R_{11\cdot 10} T_{10\cdot 9} A_{98} T_{87} S_{76} T_{60} =$$

$$= \begin{bmatrix} 1 & d_3 \\ 0 & 1 \end{bmatrix} \begin{bmatrix} 1 & 0 \\ 0 & 1 \end{bmatrix} \begin{bmatrix} 1 & d_2 \\ 0 & 1 \end{bmatrix} \begin{bmatrix} 1 & 0 \\ -\frac{1}{f} & 1 \end{bmatrix} \begin{bmatrix} 1 & d_1+R \\ 0 & 1 \end{bmatrix} \begin{bmatrix} 1 & 0 \\ -\frac{2}{R} & 1 \end{bmatrix} \begin{bmatrix} 1 & R \\ 0 & 1 \end{bmatrix} =$$

$$= \begin{bmatrix} -1-\frac{2d_1}{R}+\frac{d_2}{f}+\frac{d_3}{f} & -d_1 \\ \frac{1}{f} & 0 \end{bmatrix} \tag{9}$$

Where:

T_{60} = The ray-transfer matrix is from P_0 to P_6

S_{76} = The reflection matrix from a spherical mirror is from P_6 to P_7

T_{87} = The ray-transfer matrix is from P_7 to P_8

A_{98} = The thin lens refraction matrix is from P_8 to P_9

$T_{10\cdot 9}$ = The ray-transfer matrix is from P_9 to P_{10}

$R_{11\cdot 10}$ = The reflection matrix of a planar mirror is from P_{10} to P_{11}

$T_{12\cdot 11}$ = The ray-transfer matrix is from P_{11} to P_{12}

Thus the ray at the point P_{12} on the LCD photomask position is given by:

$$\begin{bmatrix} y_2 \\ \theta_2 \end{bmatrix} = M2 * \begin{bmatrix} y_1 \\ \theta_1 \end{bmatrix} = \begin{bmatrix} -1-\frac{2d_1}{R}+\frac{d_2}{f}+\frac{d_3}{f} & -d_1 \\ \frac{1}{f} & 0 \end{bmatrix} \begin{bmatrix} y_1 \\ \theta_1 \end{bmatrix} \tag{10}$$

If d_1 = f and y_1 =0, Eq. (10) can be simplified as

$$\begin{bmatrix} y_2 \\ \theta_2 \end{bmatrix} = \begin{bmatrix} 1-\frac{d_2}{f}-\frac{d_3}{f} & f \\ -\frac{1}{f} & 0 \end{bmatrix} \begin{bmatrix} 0 \\ \theta_1 \end{bmatrix} \tag{11}$$

Consequently, $y_2 = f\ \theta_1$ and $\theta_2 = 0$ (12)

From the results of Eqs. (8) and (12), the ray angle θ_2 on the LCD photomask is independent of the incident ray angle θ_1 in two ray trajectories. The optical system emits parallel light upwardly (θ_2 =0) through the LCD photomask to expose and solidify the photo-curable resin.

The focal length of the biconvex lens and the radius of curvature of the spherical mirror are selected for 15 cm and 10 cm due to the machine space limitations, respectively. Because the high power xenon lamp could generate enough convection and radiation heat to affect the LCD photomask and resin, a sunshade is placed between the biconvex lens and flat mirror to reduce the heat transfer to the LCD photomask.

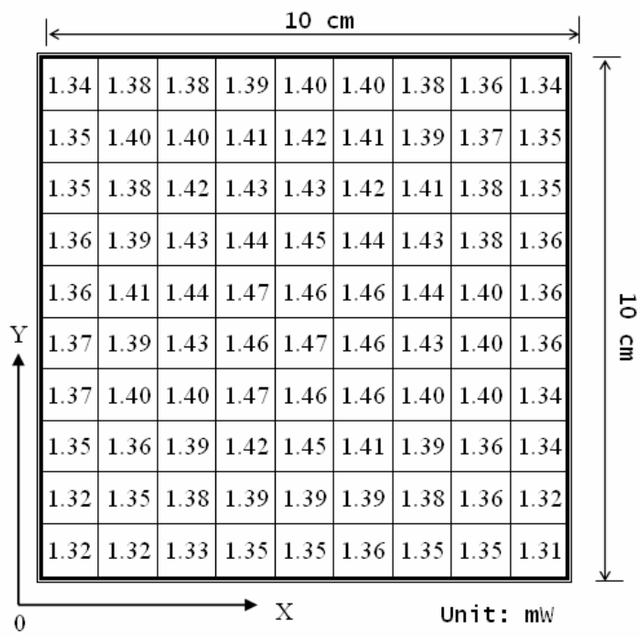

Fig. 11. The light power spreads on the LCD photomask

After constructing the optical system, measurement of the power that spreads onto the LCD photomask is necessary. This research uses an optical power meter to measure the light power that spreads onto the LCD photomask. The valid light area on the LCD photomask is 10 x 10 cm². This research divides the valid area into 100 equal parts. Each part is measured the light power using an optical power meter. The measured values are shown in Fig. 11. From these experimental results the light that spreads onto the LCD photomask is determined in good uniform. The light source uses 275W xenon lamp. The average light power through the LCD photomask is 1.43 mW.

3. Software design

3.1 The Bucket-Sorting algorithm

For most Rapid Prototyping systems, CAD models described in the .STL file format must be sliced into contours. An effective slicing algorithm is necessary for Rapid Prototyping systems. The simple approach is to intersect every facet with every slicing plane. This approach is time consuming. The Bucket sorting algorithm is used in the slicing pre-processing for search speed enhancement.

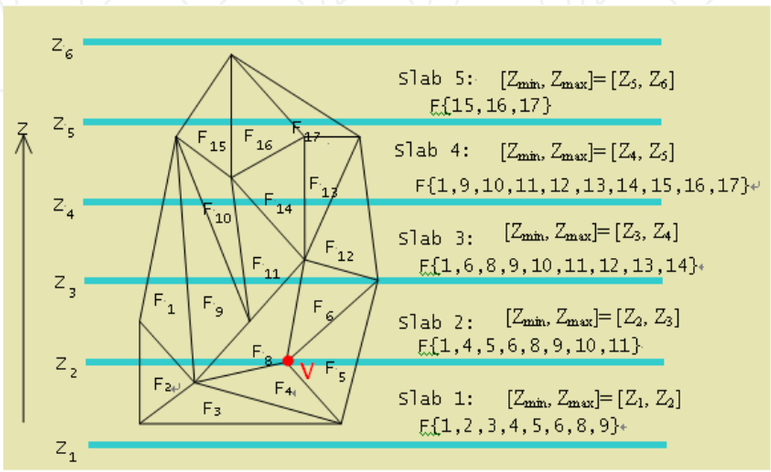

Fig. 12. The bucket-sorting algorithm for data sorting

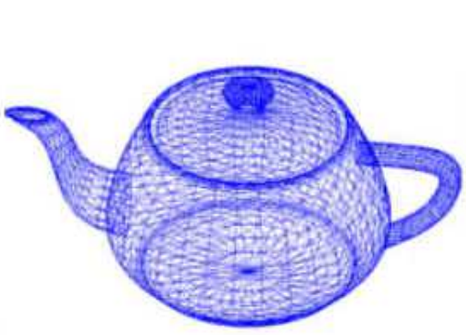

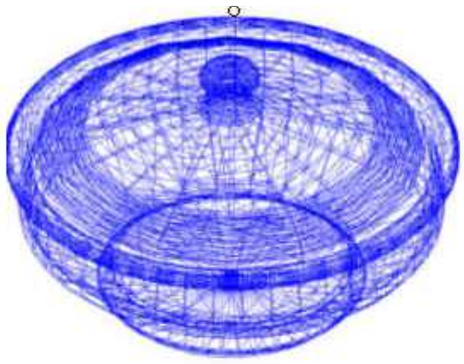

Fig. 13 (a). Fig. 13 (b).

Facet Number： 4096 Facet Number： 5192

Height range：56.114 inch Height Range：180.718 inch

Bucket number	1	5	10	20	30	40
Slicing time(sec)	49.251	13.309	8.633	6.409	5.709	5.388
Time ratio	100%	27%	17.5%	13%	11.6%	11%

Bucket number	50	60	70	80	90	100
Slicing time(sec)	5.238	5.257	5.268	5.287	5.558	5.598
Time ratio	10.6%	10.7%	10.7%	10.7%	11.3%	11.4%

Table 1. The slicing time (sec) for the different Bucket number [Fig. 13 (a).]

Bucket number	1	5	10	20	30	40
Slicing time(sec)	194.28	50.363	31.826	23.26	20.29	18.54
Time ratio	100%	25.9%	16.4%	12%	10.4%	9.5%

Bucket number	50	60	70	80	90	100
Slicing time(sec)	17.57	17.24	17.045	16.72	16.84	16.99
Time ratio	9.0%	8.9%	8.8%	8.6%	8.7%	8.8%

Table 2. The slicing time (sec) for the different Bucket number [Fig. 13 (b).]

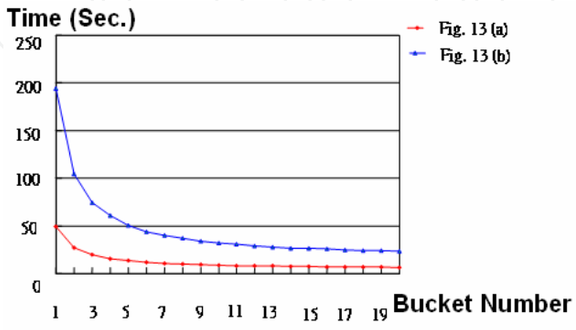

(a)

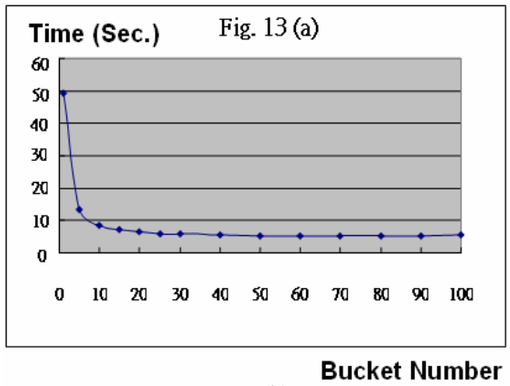

(b)

Fig. 14(a) The Slicing time for different Bucket number; Fig. 14(b) The Slicing time for different Bucket number

The bucket-sorting algorithm divides the spatial space into N subspaces. Searching for triangular data inside these smaller subspaces is often faster than browsing the entire space. In this study, the split space was also called a slab as illustrated in Fig.12. The slabs were generated by the defined maximum acceptable thickness and by the maximum and minimum Z-coordinate of the facets. Each slab was defined between a Z_{min} and a Z_{max} (Fig.12.), so that, when slicing at a specific height z, the specific slab was the one that included z within its limits [Z_{min}, Z_{max}]. A facet is assigned to a slab whenever one or more of its vertices fall within the slab's range. If a vertex has a Z value exactly equal to the boundary height between two slabs, that facet is assigned to both slabs. Fig.12 shows that the four facets (F_4,F_5,F_6,F_8) have a common vertex (V) and this vertex's Z-coordinate equals to the boundary height (Z_2) between two slabs (Slab 1 and slab 2). Consequently, these facets ((F_4,F_5,F_6, and F_8) are assigned to both slabs (slab1 & slab 2).

To implement the bucket-sorting algorithm, Figs. 13(a) and 13(b) are the input files. The Bucket number was changed to compare the slicing time. The results (slicing time) for different bucket numbers are shown in Table 1 [Fig. 13 (a).] and Table2 [Fig. 13 (b).]. If the bucket number is 1, the bucket-sorting algorithm was not used. From these results, the slicing time is greatly reduced using the bucket-sorting algorithm.
The results from Table 1 and Table2 are shown in Figs. 14(a) and 14(b). From these results, the slicing time is greatly reduced by the bucket-sorting algorithm. The slicing time ratio can be reduced by nearly 25% with 5 buckets. In Table 1, the slicing time ratio will reach the minimum value with 50 buckets. If the Bucket number is more than this certain value (50 for Table 1), the slicing time will increase. However, in Table2, the fastest slicing time will occur at 80 buckets. This optimum bucket number for slicing time is not a fixed value. It depends on the RP part's height, facet number and the size of the facets. In general, the optimum Bucket number value is 8~10. If the Bucket number is greater than 10, the slicing time will not be obviously decreased. This means that too many buckets are not useful for reducing the slicing time.

3.2 The LCD photomask display algorithm

The LCD photomask displays the cross-sectional contours of model layers and the optical system can project the light through the white areas of the photomask. The LCD photomask display algorithm is described as follows. The program fills with white color inside the contour, and fills with black color outside the contour. The light beam shines through the white areas to cure the resin. After curing one layer, the program will display the cross-sectional contour of the next layer in the LCD photomask. When all layers have been built, the program stops the RP machine and the physical part is finished.
We used Visual BASIC as the algorithm compiler. The program outputs display data to the LCD photomask to display the filled contours layer by layer. Fig. 15(a) shows a STL file which is created by Pro/Engineering 3D CAD software. Fig. 15(b) is the result after slicing the STL file. Fig. 16(a) and Fig. 16(b) show the cross-sectional contours filled with white color inside the contour.

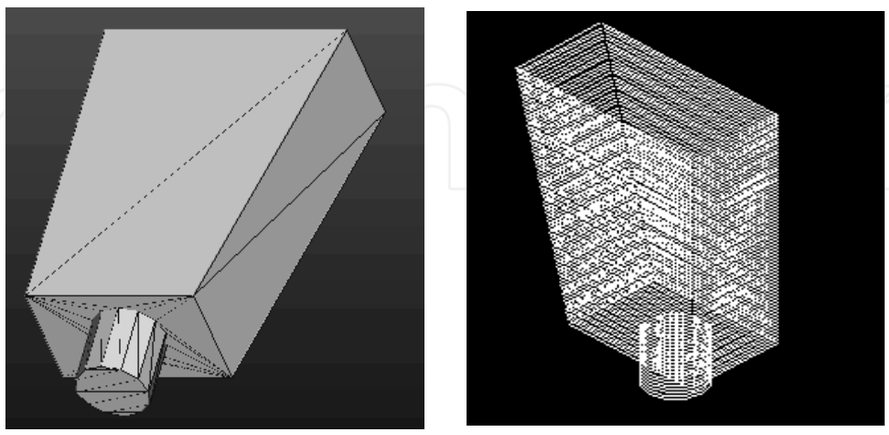

(a) (b)

Fig. 15(a) STL Model created by Pro/Engineering CAD software; Fig. 15(b) STL model sliced using the slicing process

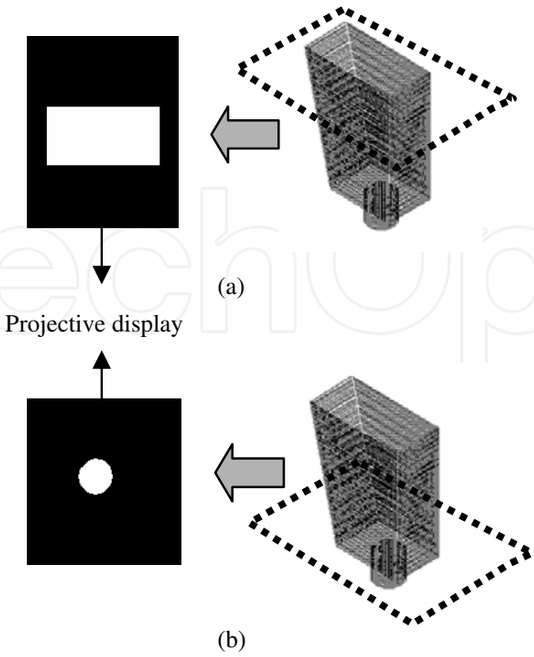

Fig. 16. LCD photomask shows the cross-sectional contours filled with white color

As described above, the proposed desktop manufacturing system uses photo-curable liquid resin NAF-200N to serve as the building material. This resin will solidify under exposure to 680 nm wavelength light. From the experimental results, the relation between the exposure time and hardened depth of the resin is illustrated in Table 3. In general, the proposed system uses uniform slicing and the layer thickness is set to 0.254mm so that the exposure time for each layer is 135 sec.

4. Experimental results

In order to compare the machining efficiency, the FDM 2000 RP machine (Stratasys Inc.) has been chosen for comparison. Although FDM 2000 is among the slowest system, it is the only RP system available in our laboratory. A 100mm x 100mm x 1mm thin plate is manufactured by the FDM 2000 and the proposed RP system. After finishing the slicing process, the tool path for FDM 2000 RP machine is shown in Fig. 17(a), and the LCD photomask display of the proposed RP system is shown in Fig. 17(b). The manufacturing time for building one layer is 582 seconds in FDM 2000. However, the manufacturing time for building one layer is 135 seconds in the proposed RP system. The machining efficiency of the proposed system is better than the FDM 2000 RP system. The accuracy of the proposed RP system is 0.4mm (0.015 inch), which is sufficient for real applications.

	1	2	3	4	5	6	7	8	9
Exposure time (sec)	15	30	45	60	75	90	105	120	**135**
Hardened thickness (mm)	0.010	0.015	0.030	0.050	0.06	0.100	0.150	0.200	**0.254**

Table 3. The experimental results: The exposure time relative to hardened depth of the resin

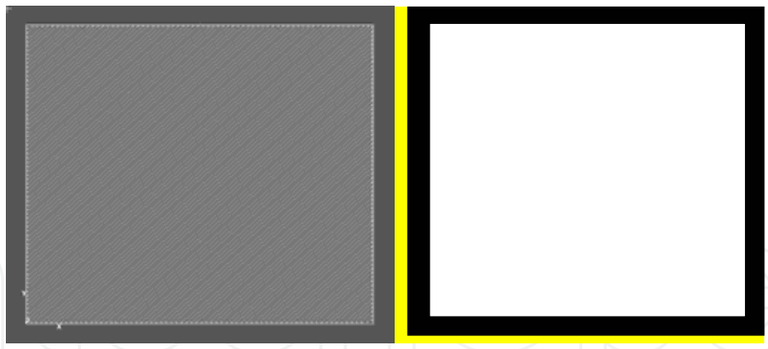

(a) (b)

Fig. 17(a) Tool path for FDM 2000 RP machine; Fig. 17(b) The LCD photomask display of the proposed RP system

4.1 Case 1

In Case 1, the 3D CAD model is illustrated in Fig. 18(a) and the STL model is shown in Fig. 18(b). The RP software reads the STL file first and proceeds with the slicing process. The sliced model is shown in Fig. 19(a).

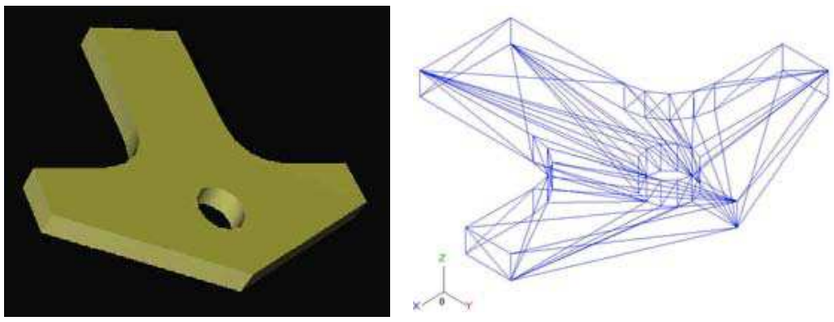

(a) (b)

Fig. 18(a) 3D CAD model of Case 1; Fig. 18(b) STL model of Case 1

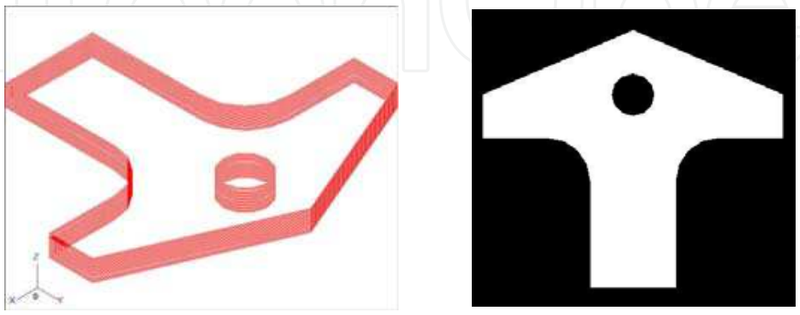

(a) (b)

Fig. 19(a) Illustration of sliced model; Fig. 19(b) Cross contour displayed in the LCD photomask

Fig. 20. RP part of Case 1 built by the proposed desktop manufacturing system

The LCD photomask displays the cross contour and the proposed desktop manufacturing system builds the physical model. The cross contour displayed in the LCD photomask is illustrated in Fig. 19(b). The physical part is built using the proposed system layer by layer. The finished RP part for Case 1 is shown in Fig. 20.

4.2 Case 2

In Case 2, the 3D CAD model is illustrated in Fig. 21(a) and the STL model is shown in Fig. 21(b). After slicing the STL file, the sliced model is illustrated in Fig. 22(a), and the LCD photomask cross contour is illustrated in Fig. 22(b). The physical part built using the proposed system is shown in Fig. 23.

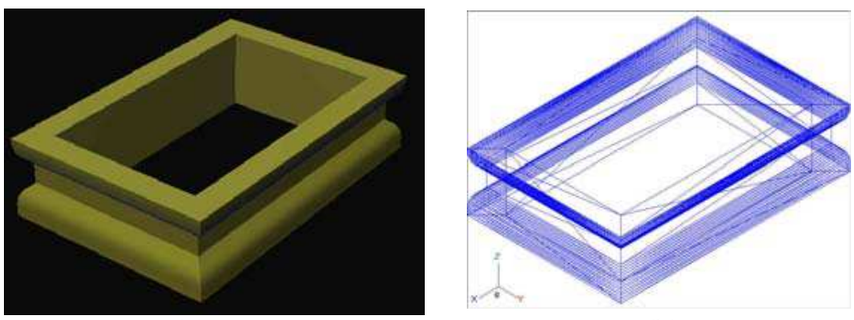

(a) (b)

Fig. 21(a). 3D CAD model of Case 2; Fig. 21(b) STL file of Case 2

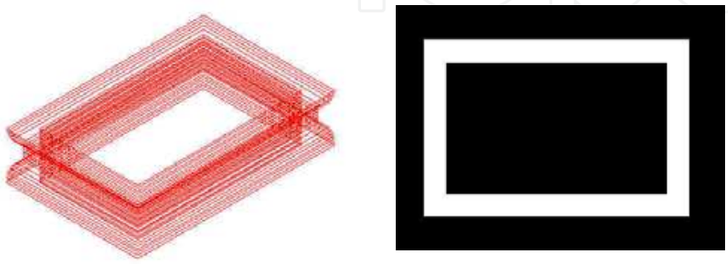

(a) (b)

Fig. 22(a). Sliced model of Case 2; Fig. 22(b) Cross contour in the LCD photomask

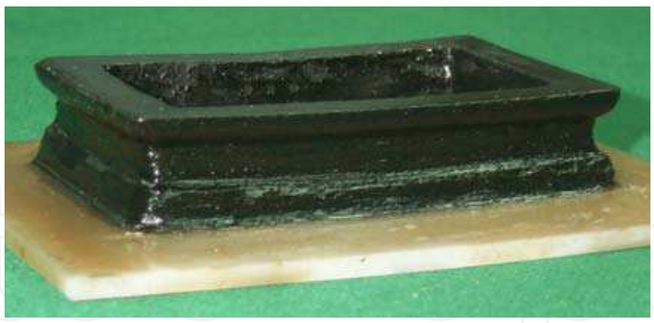

Fig. 23. RP part of Case 2 built by the proposed desktop manufacturing system

The experimental results of Case 1 and Case 2 are also shown in Table 4.

	Layer number	Layer thickness	Curing time of each layer	Total curing time
CASE 1	49	0.254 mm	135 sec	110.25 min
CASE 2	60	0.254 mm	135 sec	135 min

Table 4. The experimental results of Case 1 and Case 2

5. Conclusions

Desktop manufacturing system has been widely known as being able to fabricate 3D objects with complex geometric shapes. The purpose of this paper is to develop a LCD photomask based desktop manufacturing system. The main features of the proposed system are described as follows:

1. The LCD photomask is connected to the computer, to allow changing the cross sectional display of each layer quickly.
2. The software design includes a Slicing algorithm, LCD photomask display process, user interface and motion control program. The Bucket-sorting algorithm is used in the slicing pre-processing for search speed enhancement. The slicing time ratio can be reduced to nearly 25% with 5 buckets.
3. The hardware configuration of this architecture includes LCD photomask, optical system, z-axis elevator and PC based control system.
4. The Matrix optics is used to design the optical system.
5. The experimental results show that the proposed desktop manufacturing system can produce RP parts with good machining efficiency, but the surface roughness should be further improved.
6. The proposed desktop manufacturing system has the advantages of low cost, compactness, speed and accuracy, and requires no additional support, providing a valuable addition to the working office environment for designers at all levels and in all locations.

6. References

Bahaa E. A. Saleh and Malvin Carl Teich (1991). *Fundamentals of Photonics*, John Wiley & Sons, Inc.

Chua Chee Kai (1994). Three-dimensional rapid prototyping technologies and key development areas, *IEE Computing & Control Engineering Journal*, pp. 200 ~ 206.

Eugene Hecht, (2002). *OPTICS*, 4th edition, Pearson Education, Inc., publishing as Addison Wesley, San Francisco, CA.

Huang, Y.- M.; Jiang, C.-P. (2003). Numerical analysis of a mask type stereolithography process using a dynamic finite element method, *The International Journal of Advanced Manufacturing Technology*, Vol. 21, No. 9, pp 649-655.

Jiang, C. -P. *, J. -Y, Jeng, Y. -M., Huang and M. -J. Tsai (2005). Development of Masked Photo-polymerization Rapid Prototyping System using Liquid Crystal Display Panel, *Journal of the Chinese Institute of Industrial Engineers*, Vol. 22, No.1, pp76-81.

Luo, R. C., Tzou, J. H., and Lee, W. Z. (2000). The Development of LCD Panel Display Based Rapid Prototyping System for Advanced Manufacturing, *Proceedings* of the *2000 IEEE International Conference on Robotics and Automation*, San Francisco, CA, USA, Vol. 4, pp. 3083-3088.

Monneret, Serge; Le Gall, H.; Bade, V.; Devaux, F.; Mosset, A.; Lantz, E., (2002). Dynamic UV microstereolithography, *Applied Physics*, Vol. 6, No. 3, pp 213-218.

Prashant Kulkarni, Anne Marsan and Debasish dutta (2000). A review of process planning techniques in layer manufacturing, *Rapid Prototyping Journal*, Vol. 6, No. 1,pp. 18-35.

Puntambenker, N. Jablokow, A. and Sommer, H. (1994). A unified review of 3D model generation for reverse engineering, *Computer Integrated Manufacturing*, 7, pp259-269.

Ren C Luo and Yawei Ma (1995). A Slicing Algorithm for Rapid Prototyping and Manufacturing, *Proceedings of the IEEE international Conference on Robotics and Automation*, pp 2841-2846.

S. C. Ventura, S. C. Narang, S. Sharma, J. Stotts, C. Liu, S. Liu, L-H. Ho, D. Annavajjula, S.J. Lombardi, A. Hardy, M. Mangaudis, E. Chen, L. Groseclose (1996). A New SFF Process for Functional Ceramic Components, Proceedings of the Solid Freeform Fabrication, pp 327-334.

Soboh, T. Owen, J. Jaynes, C. Dekhil, M. and Henderson, T. (1995). Industrial inspection and reverse engineering, *Proceedings of the IEEE CAD-based Vision*, pp. 228-235.

Young, J. S. Fox, S. R. Anseth, K. S. (1999). A novel device for producing threedimensional objects, *Journal of Manufacturing Science & Engineering.* Vol. 121, No.3, pp 474-477.

http://www. 3dsystems.com/

http://www. objet.com/

http://www.envisiontec.de/index.htm

http://www.3dsystems.com/

http://www.stratasys.com/
http://www.cubital.com/

Motion Control

Edited by Federico Casolo

ISBN 978-953-7619-55-8
Hard cover, 590 pages
Publisher InTech
Published online 01, January, 2010
Published in print edition January, 2010

The book reveals many different aspects of motion control and a wide multiplicity of approaches to the problem as well. Despite the number of examples, however, this volume is not meant to be exhaustive: it intends to offer some original insights for all researchers who will hopefully make their experience available for a forthcoming publication on the subject.

How to reference

In order to correctly reference this scholarly work, feel free to copy and paste the following:

Ren C. Luo and Jyh-Hwa Tzou (2010). Development of a LCD Photomask Based Desktop Manufacturing System, Motion Control, Federico Casolo (Ed.), ISBN: 978-953-7619-55-8, InTech, Available from: http://www.intechopen.com/books/motion-control/development-of-a-lcd-photomask-based-desktop-manufacturing-system

INTECH
open science | open minds

InTech Europe
University Campus STeP Ri
Slavka Krautzeka 83/A
51000 Rijeka, Croatia
Phone: +385 (51) 770 447
Fax: +385 (51) 686 166
www.intechopen.com

InTech China
Unit 405, Office Block, Hotel Equatorial Shanghai
No.65, Yan An Road (West), Shanghai, 200040, China
中国上海市延安西路65号上海国际贵都大饭店办公楼405单元
Phone: +86-21-62489820
Fax: +86-21-62489821

IntechOpen